Photonic integration for UV to IR applications

Cite as: APL Photon. 5, 020903 (2020); doi: 10.1063/1.5131683
Submitted: 22 October 2019 • Accepted: 8 January 2020 •
Published Online: 11 February 2020

Daniel J. Blumenthal[a)]

AFFILIATIONS

Department of Electrical and Computer Engineering, University of California at Santa Barbara, Santa Barbara, California 93105, USA

[a)]Author to whom correspondence should be addressed: danb@ucsb.edu

ABSTRACT

Photonic integration opens the potential to reduce size, power, and cost of applications normally relegated to table- and rack-sized systems. Today, a wide range of precision, high-end, ultra-sensitive, communication and computation, and measurement and scientific applications, including atomic clocks, quantum communications, processing, and high resolution spectroscopy, are ready to make the leap from the lab to the chip. However, many of these applications operate at wavelengths not accessible to the silicon on insulator-based silicon photonics integration platform due to absorption, power handling, unwanted nonlinearities, and other factors. Next generation photonic integration will require ultra-wideband photonic circuit platforms that scale from the ultraviolet to the infrared and that offer a rich set of linear and nonlinear circuit functions as well as low loss and high power handling capabilities. This article provides an assessment of the field in ultra-wideband photonic waveguides to bring power efficient, ultra-high performance systems to the chip-scale and enable compact transformative precision measurement, signal processing, computation, and communication techniques.

I. INTRODUCTION

Photonic integrated circuits (PICs) enable many applications to be realized at the chip-scale and provide a path to reduced cost, complexity, power, size, and improved manufacturability. Examples include digital coherent communications,[1] fiber radio frequency (RF) transmission,[2,3] integrated microwave photonics (IMWP),[4] and positioning and navigation.[5] Emerging precision applications including atomic clocks,[6] precision metrology, and transformative applications such as quantum communications and information processing[7,8] will also benefit from photonic integration. However, many of these applications operate at wavelengths and at a level of performance not achievable with today's large scale silicon on insulator-based silicon photonic platforms.

The drive to produce high volume PICs has leveraged scaling of the silicon CMOS foundry and the associated manufacturing ecosystem.[9] The demand for silicon compatible photonics has accelerated the development of SOI-based silicon photonics, a combination of silicon on insulator (SOI)[10] and III–V[11] photonics with CMOS electronics. Both SOI and III–V photonics deliver solutions at the communication wavelengths and IR. However, for applications that operate at wavelengths shorter than 1 μm, the relatively small bandgap of silicon leads to high waveguide loss or non-transparency as well as limited power handling capabilities that occur due to nonlinear losses, primarily to two photon absorption or TPA.[12] High losses also limit the optical bandwidth of desired nonlinear optical effects, such as four-wave mixing (FWM) and second harmonic generation (SHG) that provide the ability to span the visible to IR. Examples include octave spanning and self-referenced optical frequency comb (OFC).[13,14]

A wide range of emerging applications will drive the need for new wide-bandwidth photonic integration, which offer low optical losses extending from the ultraviolet (UV) to the infrared (IR). The application space over various wavelength windows in the UV (~200 nm) to the IR (~2350 nm) regime is illustrated in Fig. 1. In addition to low linear losses, there are high performance emerging applications that require waveguides that can handle high optical power, minimizing unwanted nonlinear phase shifts and nonlinear losses. These new applications focus particularly on the UV to Near IR (NIR) range (~200 nm–900 nm). Yet at the same time, there are applications that require optical nonlinearities, and waveguide technology is required that supports desired nonlinear interactions as well as required dispersion. These nonlinear and dispersion properties must be supported at the application wavelengths of interest with some applications generating frequencies that span optical octaves. These waveguides must also support more

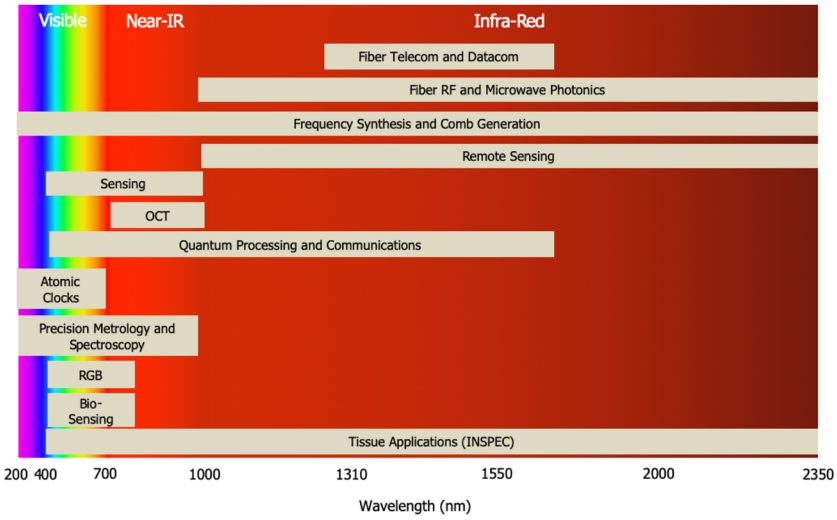

FIG. 1. Application space for ultra-wideband next generation photonics and PIC platforms.

complex functions on-chip, including low loss linear passive components (e.g., splitters, demultiplexers, and filters) and compatible on-chip optical gain mechanisms that support the UV to IR. Compatible waveguide actuation mechanisms (e.g., electro-optic, stress, and thermal) that operate across this wide bandwidth must support building blocks such as modulators, phase shifters, switches, and detectors.

It is likely in the near term that a one-size-fits-all solution for PIC technology that supports low loss, gain, actuation, and nonlinearities, spanning the UV–NIR, will not be available or at the very least difficult to realize in a wafer scale foundry compatible process. Therefore, next generation photonics will most likely support heterogeneous integration of a range of passive, active, gain, and nonlinearities across multiple material systems. These heterogeneous PIC solutions must be compatible with wafer-scale processing to provide cost effective scalable solutions.

SOI provides a 300 mm wafer-scale PIC process, based on complementary metal oxide on semiconductor (CMOS) foundry processes with an ecosystem that supports device design, fabrication, and testing geared toward high volume applications operating at wavelength above 1 μm. This platform does not meet the needs of next generation UV to NIR light photonics due to the bandgap mismatch as well as an economic mismatch with lower volume applications and more specialized requirements of visible light PICs. New end-to-end PIC platforms with next generation materials and CMOS-like design and fabrication will most likely utilize smaller wafer-scale (e.g., 200 mm) PIC processes (see Ref. 15 for example).

Gain elements provide silicon with lasing, amplification, and other gain based functions, requiring addition of other material systems including III/V,[16] which can be heterogeneously integrated with silicon.[17] For example, in the telecommunication waveband, 4 in. III–V wafers (e.g., indium phosphide) followed by hybrid SOI/III–V integration[18,19] or selective bonding of III–V to SOI or direct growth of III–V on SOI[20] are common approaches. SOI gain material systems operating at 1310 nm/1550 nm will need to be replaced with UV and UV–visible compatible semiconductor gain solutions (e.g., III-nitride)[21] as well as NIR gain materials (e.g., GaAs) for next generation UV–NIR heterogeneous integration and/or nonlinear light generation techniques such as second harmonic generation.[22]

II. NEXT GENERATION PHOTONIC INTEGRATION

Next generation wideband PIC technology will need to leverage wide bandgap semiconductors. Materials that have been reported and that can support wafer-scale and heterogeneous integration include silicon nitride (Si_3N_4),[15] tantalum pentoxide (Ta_2O_3),[23] aluminum nitride (AlN),[24,25] and aluminum oxide (Al_2O_3),[26,27] as shown in Fig. 2. Heterogeneous integration using thin film lithium niobate ($LiNbO_3$) waveguides is also possible[28] and can provide important second order nonlinearities and electro-optic modulation properties. Other possibilities include ultra-low loss etched silica waveguides and resonators[29] and the Hydex waveguide platform[30] that incorporates a dope silica core embedded in a silica cladding. Silica, $LiNbO_3$, and Hydex waveguide technologies are not the subject of this perspective.

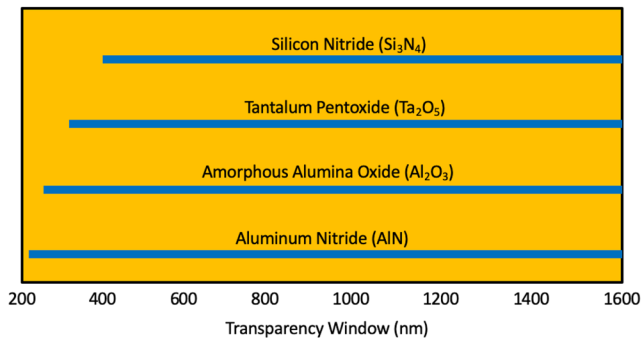

FIG. 2. Next generation optical waveguide platforms and wavelength transparency based on the bandgap: Si_3N_4,[15] Ta_2O_5,[23] Al_2O_3,[26] and AlN.[25]

Optical loss contributions, in general, are due to material absorption and waveguide scattering as well as material impurity and inhomogeneities. Thin film loss measurements help access the material absorption loss component, while actual waveguides need to be fabricated to access the waveguide scattering contributions. Other types of waveguide losses, for example, material surface effects, may contribute to losses in the waveguide core materials.

A summary of published material film and waveguide losses in the 200 nm–650 nm range, adapted from Ref. 31, is shown in Fig. 3 for Si_3N_4 waveguides,[27] Ta_2O_3 waveguides,[32] bulk AlN single crystal,[33] and atomic layer deposition (ALD) Al_2O_3 waveguides.[26]. While these data are representative of specific material and waveguide cases, a more detailed assessment of loss requires consideration of the waveguide geometry, cladding materials, mode confinement factor, device footprint, bend radius, and details of the actual fabrication process. The four materials shown have trade-offs in loss, potential waveguide geometry and optical confinement, nonlinear optical and electro-optical, and other attributes such as background autofluorescence[34] for spectroscopy applications, all of which are application dependent and can lead to choice of one material over others for reasons in addition to low loss alone. An overview of progress in low loss wide bandgap UV to IR waveguide technology is given in Ref. 27. In this paper, focus is placed on stochiometric silicon nitride deposited by low pressure chemical vapor deposition (LPCVD) due to the success of ultra-low optical losses,[15] in part due to the high temperature anneals used to remove absorbing hydrogen bonds (e.g., N–H). Other silicon nitride waveguide compositions and processes have been widely used with great success including silicon-rich nitride (SiRN)[35] to reduce stress induced cracking for thick waveguides and PECVD nitride;[36] however, these silicon nitride waveguides are not covered in this perspective article.

The Si_3N_4 material system offers transparency over an extremely wide wavelength range (~400 nm–2350 nm). The lowest reported loss designs employ a silica-based planar waveguide with a high-aspect ratio stochiometric Si_3N_4 core, low H absorption through annealing,[37,38] and a wafer bonded upper cladding to achieve a record low loss (0.045 ± 0.04) dB/m.[39] The subsequent development of a low-loss PECVD deposited upper cladding instead

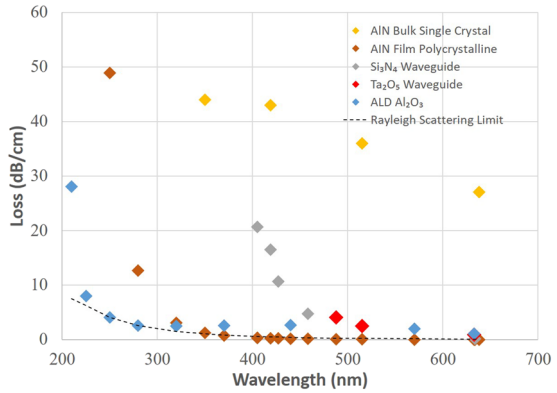

FIG. 3. Published UV to visible loss data for silicon nitride (Si_3N_4),[15] alumina (Al_2O_3),[26] tantalum pentoxide (Ta_2O_5),[32] and aluminum nitride (AlN).[33] Adapted from Ref. 31.

of wafer bonded cladding was an important step to wafer-scale manufacturable Si_3N_4 PICs with losses of ~0.3 dB/m[38] and ring resonator loaded Q factors of 30×10^6 and higher.[38,40] The Si_3N_4 waveguide system is relatively mature and can be used to fabricate complex PICs typically on 4″ or 6″ wafers.[15] Today's ultra-low loss waveguides rely on low optical confinement in the thin Si_3N_4 core suitable for large area devices with bend radius on the order 10 mm. For compact devices (sub-millimeter diameter) with a high optical mode confinement and nonlinear optical applications, processing techniques that overcome stress induced cracking for waveguide thickness greater than 400 nm and that minimize sidewall scattering losses are required.[41,42] At wavelengths close to 400 nm, Si_3N_4 bandgap material losses dominate and waveguide losses move toward 20 dB/cm or higher. This loss may be acceptable for certain applications and designs. An overview of the history of and progress in Si_3N_4 photonics is given in Ref. 15.

When operation below 400 nm wavelength is desired, the wider bandgap tantalum pentoxide (Ta_2O_3), also referred to as tantala, is a strong candidate. Tantala waveguides have shown record low waveguide losses (~3 dB/m) at 1550 nm[23] with measured losses below 5 dB/cm just below 500 nm. Transparency of this material based on the bandgap is theoretically close to 250 nm. For moderate core thickness (e.g., 90 nm), tantala loss at 1550 nm is lower than the equivalent, a 90 nm thick core Si_3N_4 waveguide. Tantala can also be deposited to make thick cores (e.g., 800 nm–1 μm) without the stress cracking issues of stochiometric Si_3N_4, making it an attractive material for ultra-compact and high optical confinement structures for applications such as optical frequency comb generation.[43] Ring resonator structures with loaded Q values in the several million have been reported.[43] Consideration needs to be given to the annealing process used to drive out hydrogen in oxide cladding to achieve ultra-low losses in silicon nitride waveguides. Tantala anneal temperatures are limited to approximately 600 °C due to material crystallization, compared to ~1200 °C that can be used for Si_3N_4. This makes it important to limit if not eliminate the presence of hydrogen during the fabrication of oxide cladded tantala waveguides. Additionally, tantala has an optical nonlinear coefficient greater than Si_3N_4,[44,45] making it an attractive material for broadband nonlinear frequency applications including optical frequency combs[43] and supercontinuum generation.[46] Tantala has other advantages for applications involving generation and detection of low levels of light like nanophotonic waveguide enhanced Raman spectroscopy (NWERS) where the level of background Raman autofluorescence is low compared to the desired Raman signal.[34]

Aluminum nitride (AlN), with much higher loss than silicon nitride and tantala, offers a bandgap that supports transparency down to wavelengths of 350 nm and shorter with the potential for UV operation. The published loss of single crystal bulk AlN down to the 350 nm wavelength[33] is shown in Fig. 3, and AlN waveguide ring resonators on the sapphire substrate with an intrinsic (different from loaded) Q of >170 000 at 638 nm and >20 000 at 369.5 nm have been reported.[24] The trade-off in higher loss for shorter wavelength operation may be desirable for certain applications. AlN also offers the important capability of electro-optic modulation and signal processing out to GHz frequencies[25] as well as second order nonlinearity. The AlN platform is one of the several discussed here that offers the exciting potential for quantum optics applications but rely on a different set of substrate and cladding materials. The AlN

TABLE I. Summary of materials, losses, and integration platform compatibility at sample wavelengths and applications.

Materials	Example wavelength/loss	Example application	Platform compatibility	References
Si_3N_4	780 nm	Rubidium atom cooling and atomic clocks	High	15
Al_2O_3	780 nm/985 nm	(Nano) waveguide enhanced Raman spectroscopy—NWERS/WERS	High	34 and 47
Ta_2O_5	633 nm	UV–VIS spectroscopy	High	48
AlN	638 nm	Quantum computing	High	24

platform is one of the three main candidates, which offers possibilities for integrated quantum optics that require operation near the UV in addition to short wavelength nonlinear optics spectroscopy.

Finally, aluminum oxide (Al_2O_3), also referred to as alumina, shows strong promise for low loss integration from the UV to visible (208 nm–633 nm). Low loss waveguides fabricated using an atom layer deposition (ALD) process[31] and sputter deposition[34] have achieved the best results with waveguide losses <3 dB/cm at the 371 nm wavelength and ring resonator intrinsic qualify factor >470 000 at the 405 nm wavelength.[24] An advantage of alumina is the low but sufficient index of refraction relative to an oxide cladding at UV wavelengths so that dilute optical modes that result in low sidewall scattering losses can be supported.

New applications will drive the demand for photonic integration platforms that support operation from the UV to IR and also drive next generation photonic integration beyond today's silicon photonic integration. These platforms will be based on wide bandgap materials and waveguide fabrication processes that provide low propagation losses. The most promising waveguide platforms are the silicon nitride (Si_3N_4), tantala (Ta_2O_3), aluminum nitride (AlN), and alumina (Al_2O_3).

A summary of materials, losses, and integration platform compatibility at sample wavelengths and applications is given in Table I.

III. LOW LINEWIDTH LASERS

Ultra-low linewidth lasers,[49] the mainstay of high-end scientific experiments and applications, will benefit greatly from next generation photonics. Translating the performance of these spectrally pure lasers to wafer-scale integrated devices will bring lower cost, size, weight, and power along with increased environmental robustness to applications that are today confined to the laboratory. Realizing lasers with this level of performance, which produce ultra-low linewidth across the visible to IR, will require wide bandwidth photonics. These applications include coherent communications,[1] next-generation data center interconnects,[50] atomic and quantum sensing,[51,52] atomic clocks,[6] precision metrology and time-frequency transfer,[53] and quantum communications and computation.[7,8] Other applications include microwave frequency synthesizers[54] and optical laser gyros.[55]

The stimulated Brillouin scattering (SBS) laser[56] is an important laser class capable of producing highly coherent, spectrally pure emission that can operate from the visible[57] to the infrared.[58] With sub-hertz fundamental linewidth and the capability for hertz level integral linewidth emission through cavity stabilization,[59–62] this class of laser is an ideal candidate for integration. Brillouin is an elegant nonlinearity, based on interaction between sound and light, and can support wide bandwidth lasing from visible to infrared.

There has been significant progress toward the integration of the SBS laser, historically limited to fiber implementations, into a photonic integrated platform, as summarized in Fig. 4. The

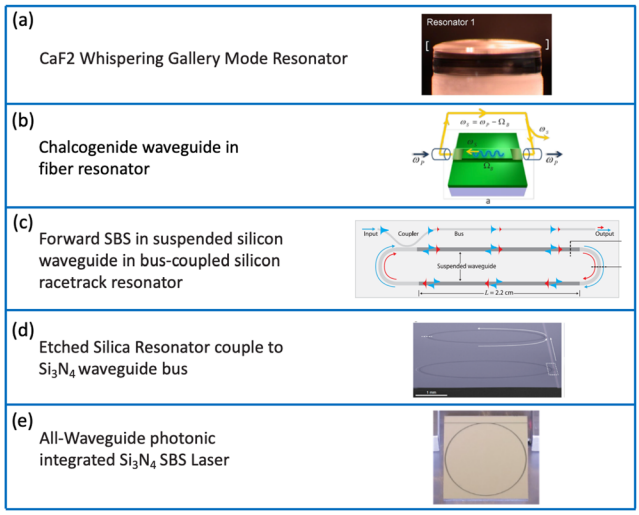

FIG. 4. Evolution of ultra-low linewidth Stimulated Brillouin Scattering (SBS) lasers from chip-scale to all waveguide photonic integrated: (a) CaF_2 whispering gallery mode resonator.[63] Reproduced with permission from Grudinin *et al.*, Phys. Rev. Lett. **102**(4), 043902 (2009). Copyright 2009 American Physical Society. (b) Chalcogenide waveguide embedded in a fiber resonator.[64] Reprinted with permission from Kabakova *et al.*, Opt. Lett. **38**(17), 3208–3211 (2013). Copyright 2013 The Optical Society. (c) Suspended silicon etched waveguide embedded in a silicon waveguide bus-coupled resonator.[65] Reprinted with permission from Otterstrom *et al.*, Science **360**(6393), 1113 (2018). Copyright 2018 AAAS. (d) Etched silica resonator coupled to an on-chip silicon nitride bus waveguide.[29] Reprinted with permission from Yang *et al.*, Nat. Photonics **12**(5), 297–302 (2018). Copyright 2018 Macmillan Publishers Ltd. (e) Photonic integrated all-waveguide Si_3N_4 bus coupled resonator SBS laser.[66]

underlying principle falls into two general categories, designs that involve waveguides that are engineered to phase match the light (photons) with the acoustic (phonon) waves and designs that do not require this phase matching. The latter involves non-confined short-lived acoustic waves that are generated in a high Q resonator.

Early micro-optical SBS lasers incorporated free-space coupled CaF2 whispering gallery mode resonators capable of sub-hertz fundamental linewidth emission.[63] Moving an SBS laser to on-chip required fabrication of integrated waveguide structures that demonstrated sufficient Brillouin gain and low loss structures to fabricate a high Q resonator. Chalcogenide (As_2S_3), a material with extremely high Brillouin and Kerr nonlinearities, was notably the first material used to demonstrate SBS gain in a waveguide[67] and was subsequently embedded in an external optical fiber resonator to demonstrate SBS lasing.[64] Brillouin gain was later demonstrated in a suspended silicon waveguide[68] and an SBS laser demonstrated by embedding the suspended waveguides in an integrated silicon waveguide bus-coupled racetrack resonator.[65] Chemically etched silica resonators coupled to a tapered-fiber coupled chemically etched ultra-high Q silica microresonator[69] were implemented as an on-chip air clad etched silica microresonator coupled to an integrated Si_3N_4 waveguide bus.[29] These prior works required dispersion engineering between optical and acoustic modes or nonlinear absorption in the UV and visible (for silicon) making wide bandwidth operation, even with materials that have low loss, difficulty, and other limitations related to the wafer-scale compatibility of the fabrication process. By utilizing wide bandwidth Si_3N4 waveguides designed to support dilute optical modes and high power handling capability, an all-waveguide wafer scale SBS laser was recently demonstrated, showing that on-chip record sub-hertz fundamental linewidth emission[66] is possible. By realizing spectrally pure SBS lasers in a wide bandgap integration platform that also supports integration with a wide variety of components,[15] paves the way to integrated ultra-low linewidth SBS lasers for a wide range of UV to IR applications. A history of SBS photonics is given in a recent review article.[70]

IV. OPTICAL FREQUENCY COMBS

A key building block is the optical frequency comb (OFC), a single source of multiple well-defined, stable, evenly spaced frequencies.[71] Wide bandgap semiconductors have been critical toward realizing chip-scale OFCs with the capability to produce hundreds of frequencies that span tens of terahertz.[72–75]

Further integration of OFCs with other components will enable a wide range of precision applications traditionally relegated to bench-top systems. Example applications include low noise microwave frequency generation,[76] astro-combs,[77] atomic clocks,[62] spectroscopy and laser sensing, waveform synthesis,[78] and optical metrology. The large multi-octave comb emission and the ability to lithographically define combs with different line spacing and other nonlinearities such as second harmonic generation makes OFCs central to precision microwave readout using self-referencing techniques[79] to create a precision "optical ruler."[71] Wide bandgap semiconductor OFCs enable comb lines emitted at the low-frequency IR side of the emission spectrum to be referenced to comb lines at twice the frequency on the high-frequency visible side of the emission spectrum. The OFC spectral line spacing and its common offset can be locked to a radio frequency standard to create these optical rulers. Other advantages of integrated OFCs include realizing combs with spacing >100 GHz, difficult to achieve with non-integrated comb techniques. Phase stabilization for microwave synthesis using interlocking frequency combs[76] is another key application of this technology. In the fiber communication world, integrated comb generators can replace large arrays of power hungry wavelength division multiplexing (WDM) lasers for high capacity fiber communication systems[80] and the rack-scale to the chip-scale leveraging progress in next generation wide bandgap photonics.[73,81]

The basic OFC structure is, in principle, relatively simple, a bus-coupled ring resonator with the correct optical nonlinear and dispersive properties. Dissipative Kerr soliton (DKS) micro-resonator comb generators[82,80,73,81] are an important type of OFC that has found applications to frequency synthesis,[78] terabit optical communications,[80] and dual-comb spectroscopy.[83] Kerr OFCs balance nonlinear four-wave mixing parametric gain, cavity loss, and dispersion in a micro-resonator to generate continuously circulating stable soliton pulses that yield a low noise frequency comb output. There have been a wealth of successful designs realized in the Si_3N_4 waveguide platform. The absence of nonlinear losses in the wide bandgap semiconductors, such as two-photon absorption in silicon, enables these comb generators to bridge the visible to IR. Given the flexibility in Si_3N_4 to design a wide range of low loss waveguide resonators with different FSRs, the comb generator line spacing can be optimized for a given application.

Producing frequency combs that extend to the visible regime has proved more difficult. Typical combinations of parametric Kerr nonlinear processes (χ^3) in the IR are combined with second harmonic generation (χ^2) in Si_3N_4[84] and AlN waveguide resonators.[85,86] An example of visible light comb production is shown in Fig. 5 for an AlN waveguide resonator with a first nonlinear process,

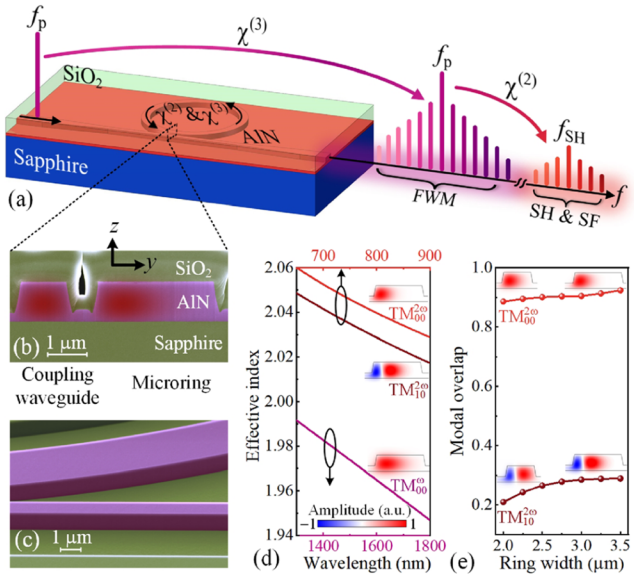

FIG. 5. Visible comb generation via (χ^2) and (χ^2) in AlN on a sapphire waveguide resonator. Reproduced with permission from Liu *et al.*, Appl. Phys. Lett. **113**(17), 171106 (2018). Copyright 2018 AIP Publishing LLC.

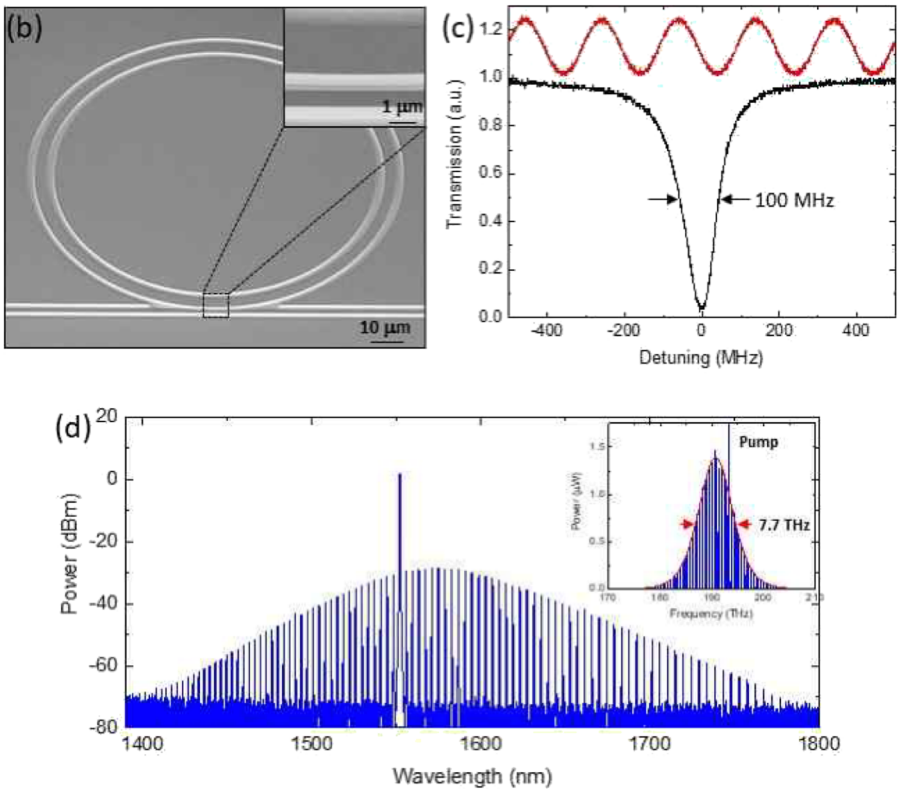

FIG. 6. Tantala Kerr nonlinear optical frequency comb.[43] From Jung *et al.*, *Nonlinear Optics (NLO)*. Copyright 2019 Optical Society of America. Reprinted with permission from Optical Society of America.

four wave mixing (FWM) comb production, followed by a second nonlinear process, second harmonic generation. Looking forward, there is much progress to be made in visible light combs in other lower loss wide bandgap semiconductors, e.g., Si_3N_4, alumina (Al_2O_3), and tantalum pentoxide (Ta_2O_5), which generate directly in the visible and bridge the UV to IR. Progress in visible to near infrared (NIR) supercontinuum light generation in Si_3N_4 has shown promise for ultra-broadband frequency generation.[13]

As an example of progress toward combs in visible capable wide band materials, the wide bandgap tantala platform has been used to demonstrate a Kerr soliton waveguide OFC with a resonator loaded Q factor of $>3 \times 10^6$ (see Fig. 6).[43]

Tantala provides low loss,[23] an index of refraction comparable to silicon nitride and a nonlinear Kerr coefficient several times larger than Si_3N_4.[23] The low stress of the deposited tantala films provides the ability to fabricate a thick waveguide structure, ~ 1 μm, needed to engineer and balance nonlinearities with group velocity dispersion (GVD) without the cracking issues of Si_3N_4. The wide bandgap of tantala offers the potential to move operation of nonlinear and linear ring resonators to the 300 nm wavelength operating regime. Initial results with tantala Kerr soliton OFCs have shown operation from 1.4 μm to 1.8 μm.

An intriguing application of wide bandgap nonlinear frequency combs is quantum information processing. Optical quantum frequency combs,[87–90] or "quantum combs," are the single photon counterpart to classical OFCs. Quantum optical computations benefit from having many entangled photon pair modes. A quantum OFC can produce many frequency modes, leveraging the wavelength parallelism of the comb teeth produced by single photon highly correlated nonlinear processes such as spontaneous four-wave mixing (SFWM).[91] An example of a processing chip for multi-photon entangled state quantum processing using an OFC is shown in Fig. 7. This approach shows promise for integrating a high number of entangled modes on a chip, using techniques such as FWM signal and idler interferometers and single photon detectors for quantum processing.[87]

Quantum information processing can benefit from the frequency teeth spacing >100 GHz achievable with integrated OFCs,

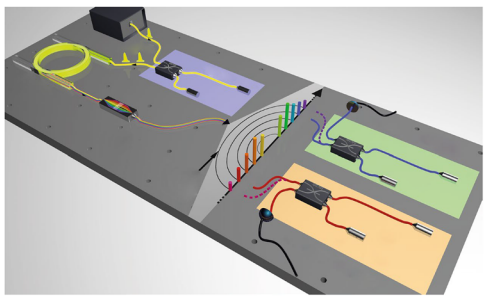

FIG. 7. Quantum OFC to generate parallel entangled mode pairs.[87] Reprinted with permission from Kues *et al.*, Nat. Photonics **13**(3), 170–179 (2019). Copyright 2017 Macmillan Publishers Ltd.

making processing of photons (e.g., filtering) manageable, whereas fiber quantum frequency combs produce narrow frequency spacing making filtering and other tasks difficult. An issue with increased spacing using integrated OFCs is the reduction in number of frequency quantum modes limited to a certain wavelength band (e.g., C-band). In order to provide more quantum modes, SFWM Kerr waveguide OFCs that extend from the visible to IR with thousands of modes such as that reported in Ref. 84 or further progress with DKS OFCs that span the visible to IR will be needed.

V. MULTI-COUPLED RESONATORS AND PHOTONIC MOLECULES

Combining multiple optical resonators into linear chains or two dimensional arrays opens up possibilities in optical signal processing, spectral engineering, and linear and nonlinear optics. Research in photonics molecules seeks to use photons in optically coupled resonant microstructures to realize functions and behaviors analogous to electronic atomic and molecular systems.[92,93] In this sense, optical resonators can be thought of as photonic atoms and collections of photonic atoms can be designed to act like photonic molecules (PMs).

Photonic molecules have the potential to impact a wide variety of UV to IR applications. Example applications include lasers for communications and sensing, spectral engineering,[92,93] optical signal processing,[92,94] nonlinear optics,[95] sensing and manipulation of small biological samples, nano-particle detection,[96] label-free single molecule detection,[97] ultra-low power optical switching,[98,99] and many body physics simulations.[100,101] Integrated resonators fabricated with wide bandwidth photonics that can achieve high loaded Q and can be fabricated into arrays will impact the field of photonic molecules and their applications.

As illustrated in Fig. 8, a single bus coupled resonator [Fig. 8(a)] behaves like an atom in resonance linewidth. Stability will not be that of an atom unless locked to an atomic resonance. Passive or active locking can lead to very stable optical resonances.[102] The bus coupled resonator is also known as an optical all-pass filter function. Two coupled resonators [Fig. 8(b)] behave like a diatomic molecule with six energy super-modes.[103] Coupling between optical cavities using quantum dots and micro-disc resonators has been shown to yield molecular behaviors like frequency splitting and bonding and anti-bonding orbitals.[98] Attractive and repulsive forces between optical resonators similar to Coulomb forces in electronic molecules can be demonstrated and utilized as well as ultrafast optical switching[104] effects and functions. An assembly of mutually coupled photonic atoms (e.g., micro-resonators) can realize a photonic molecule with modes and behave very much like their electronic counterparts with atomic energy or resonant states and molecular super-modes.[105]

A linear array of bus coupled resonators [Fig. 8(c)] lead to the formation of optical crystal bands,[106] also analogous to a thin film filter. Properties of the linear array can be designed by varying the coupling strength and sign.[107] Forming a 2D array of resonators with a line defect leads to the well-known photonic crystal [see Fig. 8(d)] structure with discrete allowable energy states and forbidden bandgaps,[108] enabling dispersion engineering and slow light[109,110] as well as other devices and functions that take the advantage of these properties (e.g., ultra-compact optical filters[111,112]). By varying the size of the coupled resonators in a 2D array [see Fig. 8(e)], the photonic equivalent of defect states[113] as well as defect states in a linear resonator chain[114] can be realized.

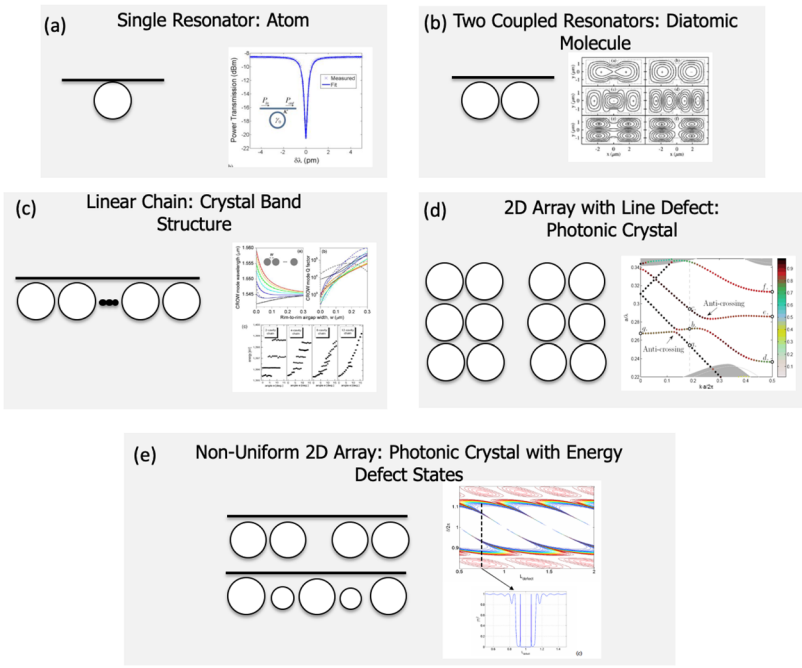

FIG. 8. Atom and molecular like properties of optical resonators. (a) A single bus-coupled resonator has the property of an atom-like mode. (b) Dual coupled resonators share similar properties with diatomic molecules. (c) Linear resonator chains resemble crystalline band structures. (d) 2D resonator arrays with a line defect form a photonic bandgap, and (e) intra-band defect states can be introduced by varying the size of the 2D resonators.

VI. OTHER WIDE BANDGAP OPTICAL COMPONENTS

Waveguide actuation and dynamic active components like modulators are critical for generating sideband control signals for feedback loops, e.g., Pound Drever Hall (PDH) stabilization,[61] and for RF analog modulation and digital data modulation. Progress in wide optical bandwidth photonic modulators has been limited. Electro-optic and strain modulations are the primary effects employed but tend to be either weak or bandwidth limited with good progress in AlN and silicon nitride. The Pockels effect was employed for electro-optic modulation in AlN to demonstrate modulation up to 4.5 Gb/s.[25] Electro-optic modulation in an AlN waveguide was employed to demonstrate a push–pull Mach-Zehnder Interferometer (MZI) modulator with 21 V Vπ at 1550 nm and 12.9 V Vπ at 1064 nm. A modulation rate of 140 MHz with a 12 dB extinction ratio (ER) was shown for the MZI, useful for signal processing and feedback loops, and a dual-ring modulator was shown to operate at 4 GHz with 3 dB ER. The stress optic effect has been employed for MHz modulation speeds using ferroelectric lead zirconate titanate (PZT) films on Si_3N_4 waveguides with MHz response RF modulation response[115] and low energy modulation for 780 nm light at cryogenic temperatures.[116] Higher speed electro-optic modulation in the O-band and C-band was achieved with PZT films deposited on Si_3N_4 bus-coupled ring modulators demonstrating modulation >25 GHz with a half-wave voltage-length product of ~1 V cm[117] Slower tuning and switching are achievable with thermally controlled actuators in many of these wide bandgap photonics, for example, Si_3N_4.[15]

The performance of demonstrated thermal, Pockels, and PZT actuators is satisfactory for relatively low bandwidth RF communication links and switching applications, e.g., quantum heralding and optical phase array switchable delay lines.[118] Other active and passive components have been demonstrated in wide bandwidth photonics;[15,27,31] however, many open issues remain as well as performance progresses especially for modulators and switches.

VII. APPLICATIONS

Applications that benefit from low loss across the visible to IR will also leverage the linear and nonlinear properties as well as ability to integrate high performance passive and active components and support traditional RF and digital system requirements as well as next generation quantum, sensing, and metrology applications.

RF optical communications, radar systems, and RF optical signal processing require complex, low loss, and high performance optical filters to shape the spectral or temporal contents as well as optimize the optical signal to noise ratio (OSNR) and perform other signal processing functions in the radio-frequency (RF) (~300 kHz–300 GHz) and microwave (~300 MHz–300 GHz) domains. Low loss, ability to support high optical powers, and high linearity are critical features for replacing power hungry electronics and maintaining transmission integrity in RF optical links. Optical filters that can handle high power before exhibiting nonlinear loss and filter distortion and that cover the multiple wavebands from visible to infrared will be indispensable for systems that combine RF and sensor systems.

A third order low loss Si_3N_4 coupled-resonator optical waveguide (CROW) filter[38] demonstrated an ultra-high 80 dB extinction ratio (ER) with low insertion loss (<1.3 dB) and a flat passband. Filters with this level of ER and filter shape performance can be used for nonlinear pump-signal separation in Brillouin, four-wave mixing (FWM), second order nonlinear generation and in precision spectroscopy. Filter channelization for RF photonic and WDM optical communications, where individual channel bandwidths can be tuned in addition to center frequency tuning, is possible with Si_3N_4 due to low loss elements. The fabricated CROW-based bandpass filter can select a channel in a frequency-division subcarrier satellite communication system.[119] Programmable RF filter networks leverage Si_3N_4 low loss to realize networks of tunable filter arrays, enabling multiple dynamically configurable complex filter functions on the same chip to implement a wide class of filter types [e.g., finite impulse response (FIR) and infinite impulse response (IIR)].[120] Programmable multistage lattice filters for dispersion compensation[121] and other analog signal conditioning applications are possible due to the ability to integrate multiple low loss elements, such as switches and delay lines, on the same chip. These programmable elements can deliver low loss and low linearity needed for many RF optical systems.

Optical delay lines are used in a wide variety of applications including RF and digital filtering, optical beam forming, optical signal processing, information coding, digital data storage and synchronizers, and pulse shaping. Non-resonant delays are used for RF and analog functions in such as transversal and FIR filters, IIR filters, and other discrete time signal processors.[122] Broadband Si_3N_4 delays provide discrete, medium to large delays, up to 250 ns on a single chip (tens of meters in length). Resonant delay lines, such as optical ring resonators (ORRs), are more compact and are continuously tunable over ranges of picoseconds to order of nanoseconds.[123] Non-resonant Si_3N_4 waveguides provide about 12.5 ns per meter delay and lengths up to 25-m with 250 ns delay have been fabricated. Spiral geometries with waveguide crossovers on a large area chip (2 cm × 2 cm)[124] have been demonstrated for applications such as optical gyroscopes.[125] Larger true time delays are possible for phased array antenna applications by combining long delay lines with Si_3N_4 optical switches.[126] Next generation signal processing elements and delay lines will see further size reduction and integration using advanced techniques such as SBS in wide bandgap photonics.[70]

In the digital application space, some of the more difficult problems today are found in the fiber data center interconnect (DCI) environment where exploding data center capacity pushes traditional fiber interconnects to their power and space limitations. The power and engineering limitations that DCIs are facing are due to the evolution of switch application specific integrated circuit (ASIC) chips, the engines of the Data Center Interconnect (DCI). Switch ASICs will grow from 12.8 Tbps today to 100 Tbps, placing a strain on energy resources[127] and traditional engineering approaches. Continued scaling of today's fiber transmission technologies in the DCI requires novel solutions and technologies. Solutions will involve bringing high capacity coherent WDM into the DCI. However, coherent WDM links rely on power consuming technologies such as digital signal processors (DSPs) and large-bandwidth phase locked loops.[128] Solutions incorporating high-capacity WDM links will have to be free of DSPs and other high power analog or digital electronics.

A new WDM coherent link architecture utilizes capacity and power scaling advantages of highly integrated, ultra-stable, narrow-linewidth laser, and transceiver technology. The ARPA-e funded

FREquency Stabilized Coherent Optical (FRESCO) project supports coherent Tbps transmission per wavelength and scaling to support future 100 Tbps switch ASICs with order several pJ per bit efficiency. FRESCO brings narrow linewidth and laser stabilization technology developed for frequency standards[61] and atomic clocks[6] to the coherent fiber DCI. The FRESCO architecture is based on a shared ultra-stable, spectrally pure laser using wide bandgap photonics to realize an ultra-stable, spectrally pure, and shared optical comb [transmit (Tx) and local oscillator (LO) source] that is modulated with a highly integrated silicon photonic coherent transceiver. A high level illustration of the FRESCO integrated transceiver is shown in Fig. 9. A FRESCO shared optical source consists of a silicon photonic tunable laser that serves as a pump for a silicon nitride SBS laser.[66] The SBS laser is stabilized to an ultra-high Q factor frequency stabilized resonator that reduces the SBS emission integral linewidth and stabilizes the optical carrier frequency and phase. The stabilized ultra-low linewidth SBS laser output pumps a nonlinear optical frequency comb (OFC) source[78] that serves as a shared WDM Tx and LO source for a multi-channel silicon photonic coherent modulator and receiver.[10]

Other application for wide bandgap next generation photonics will leverage the ultra-low phase noise and high level of integration including microwave synthesis,[54] optical gyroscopes,[130,131] and photonic quantum circuits[8] for quantum information processing and communications.[132]

An intriguing emerging chip-scale application is atom cooling.[62,133,134] Atomic clocks are constructed using tightly coordinated sets of free-space laser beams and bulky optics to cool, pump, and probe an atomic species. Certain quantum information processing architectures are based on cooled atoms. Wider deployment of atomic clocks will require the integration of the lasers and optical interfaces to reduce cost, size, and power consumption and decrease sensitivity to environmental conditions. To drive down the cost and complexity as well as improve the robustness of these systems, PICs will be required to interface pump and probe lasers, delivered by optical fibers, to free-space beams with required geometry and beam quality. Such PICs pose unique integration challenges including low loss visible light fiber-coupled waveguides, visible light passive components including splitters and combiners, and low loss

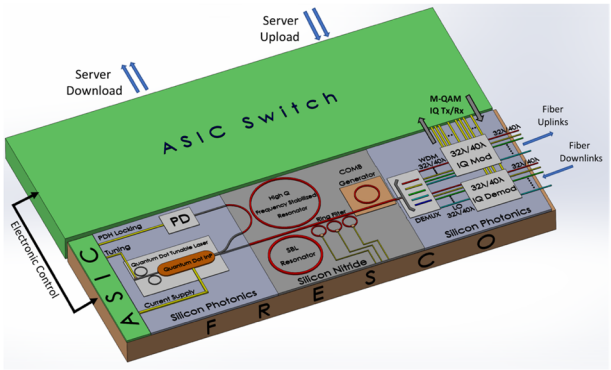

FIG. 9. FRESCO frequency stabilized ultra-low linewidth switch ASIC multi-Tbps fiber optical transceiver. Reprinted with permission from Blumenthal *et al.*, *2019 IEEE Optical Interconnects Conference (OI)*. Copyright 2019 IEEE.[129]

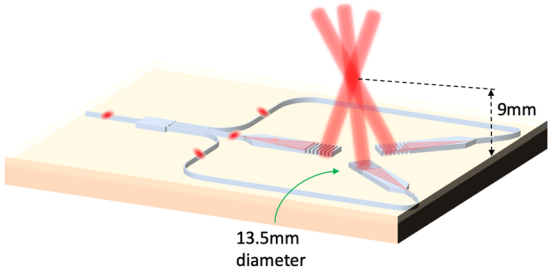

FIG. 10. Photonic integrated waveguide to free-space 3D atom cooling laser interface photonic integrated circuit (PIC). From Chauhan *et al.*, *Conference on Lasers and Electro-Optics*. Copyright 2019 Optical Society of America. Reprinted with permission from Optical Society of America.[133]

waveguide-to-free-space ultra-large-area gratings uniformly fabricated over millimeter-scale areas that emit non-diverging beams at pre-designed angles.

Recently, the design, fabrication, and measurement of a Si_3N_4 photonic integrated circuit (PIC) that interfaces a fiber-coupled 780 nm laser to serve as laser cooling beams for a 3D magneto-optic trap (3D-MOT)[135] were reported. The 3D laser cooling beam interface PIC is shown schematically in Fig. 10. A 780 nm laser is coupled via a single mode fiber to a single mode waveguide at the Si_3N_4 PIC input. The input guided light is directed to a 1 × 3 multimode interference (MMI) waveguide splitter and routed to three slab waveguide beam expanders, which, in turn, uniformly illuminates three large-area free-space surface grating emitters. The gratings are located on a 13.5 mm diameter circle and emit free-space collimated 780 nm beams, emitted at 54.7° from the PIC surface-normal, in order to produce 90° intersection between all three beams at a distance of 9 mm from the chip surface (in the center of the atom vapor cell). The large area gratings are designed to deliver free-space collimated beams to cool of a large volume of Rb-87 atoms as well as provide a good beam intensity uniformity for all six cooling beams.

VIII. SUMMARY AND FUTURE PROSPECTS

Next generation photonics will employ wide bandgap semiconductor PIC technology. Among the most intriguing platforms that support wafer-scale and heterogeneous integration are silicon nitride (Si_3N_4), tantalum pentoxide (Ta_2O_3), aluminum nitride (AlN), and aluminum oxide (Al_2O_3). These wide bandgap technologies bring to the designer's toolbox an integration platform capable of addressing key performance features not available in SOI and other platforms including ultra-low linear and nonlinear losses, transparency from the UV and visible through the infrared, and high power handling capabilities. A wide array of passive, active, linear, and nonlinear components can be combined on-chip, bringing high performance systems to the chip scale and has the potential for new signal processing, computation, and sensing systems-on-chip. Low linewidth lasers, multi-octave spanning self-referenced frequency combs, ultra-high Q resonators, and programmable optical filter networks show promise for photonic circuits that can address high bandwidth problems that are becoming too power-intensive for analog and digital electronic processing. Emerging applications

will leverage the ultra-low phase noise in including photonic quantum circuits for quantum information processing and communications and precision timing and quantum metrology using atom cooling.

Problems that remain to be tackled include the development of a true integration PIC platform that can support UV–NIR applications and wavelength specific designs without platform modifications as well as full foundry compatibility. Heterogeneous gain across the full UV–NIR range is a major issue that needs to be addressed with promise for great advances. Gain for lasing and periodic signal boosting (e.g., SOAs) that span this wavelength range and enable direct signal boosting or amplification of non-linear generated frequencies (e.g., SHG) will be critical. Other milestones to be reached include to further lower losses by another order of magnitude and reach waveguide ring resonator quality factors (Q) >100 $\times$ 10^6 heading to 1 $\times$ 10^9, down to the UV. Another critical area includes platform compatible actuation, particularly modulation. A wide range of modulation frequencies, both narrow band and broad band, are needed. At the low end (e.g., 1 MHz–500 MHz), techniques such as acousto-optic modulation (AOM) will be needed to sweep frequencies with high conversion efficiency. Signal and data modulation at high RF frequencies (>25 GHz) and high bit rates (>25 Gbps) will also be needed. With increased sensing and atom interaction applications, techniques to bring atomic and molecular materials onto these chips will be combined with ultra-low loss materials.

ACKNOWLEDGMENTS

This material is based upon work supported by the National Science Foundation under EAGER Grant No. 1745612, the DARPA MTO ACES program under Contract No. HR0011-16-C-0122, the DARPA and Space and Naval Warfare Systems Center Pacific (SSC Pacific) PRIGM/AIMS program under Contract No. N66001-16-C-4017, and the Advanced Research Projects Agency-Energy (ARPA-E), U.S. Department of Energy, under Award No. DE-AR0001042. The views, opinions, and/or findings expressed are those of the author(s) and should not be interpreted as representing the official views or policies of the Department of Defense or the U.S. Government.

REFERENCES

[1] K. Kikuchi, "Fundamentals of coherent optical fiber communications," J. Lightwave Technol. **34**(1), 157–179 (2016).
[2] C. H. Cox and E. I. Ackerman, "Microwave photonics: Past, present and future," in 2008 International Topical Meeting on Microwave Photonics jointly held with the 2008 Asia-Pacific Microwave Photonics Conference, 2008.
[3] J. Capmany and D. Novak, "Microwave photonics combines two worlds," Nat. Photonics **1**, 319 (2007).
[4] D. Marpaung *et al.*, "Integrated microwave photonics," Laser Photonics Rev. **7**(4), 506–538 (2013).
[5] G. A. Sanders *et al.*, "Fiber optic gyro development at Honeywell," Proc. SPIE **9852**, 985207 (2016).
[6] A. D. Ludlow *et al.*, "Optical atomic clocks," Rev. Mod. Phys. **87**(2), 637–701 (2015).
[7] O. Adeline and D. Eleni, "Recent advances on integrated quantum communications," J. Opt. **18**(8), 083002 (2016).
[8] F. Flamini, N. Spagnolo, and F. Sciarrino, "Photonic quantum information processing: A review," Rep. Prog. Phys. **82**(1), 016001 (2018).
[9] T. Pinguet *et al.*, "High-volume manufacturing platform for silicon photonics," Proc. IEEE **106**(12), 2281–2290 (2018).
[10] C. Doerr, "Silicon photonic integration in telecommunications," Front. Phys. **3**, 37 (2015).
[11] M. Smit *et al.*, "An introduction to InP-based generic integration technology," Semicond. Sci. Technol. **29**(8), 083001 (2014).
[12] N. Singh *et al.*, "Octave-spanning coherent supercontinuum generation in silicon on insulator from 1.06 μm to beyond 2.4 μm," Light: Sci. Appl. **7**, 017131 (2018).
[13] H. Zhao *et al.*, "Visible-to-near-infrared octave spanning supercontinuum generation in a silicon nitride waveguide," Opt. Lett. **40**(10), 2177–2180 (2015).
[14] D. R. Carlson *et al.*, "Self-referenced frequency combs using high-efficiency silicon-nitride waveguides," Opt. Lett. **42**(12), 2314–2317 (2017).
[15] D. J. Blumenthal *et al.*, "Silicon nitride in silicon photonics," Proc. IEEE **106**(12), 2209–2231 (2018).
[16] T. Komljenovic *et al.*, "Photonic integrated circuits using heterogeneous integration on silicon," Proc. IEEE **106**(12), 2246–2257 (2018).
[17] O. Marshall *et al.*, "Heterogeneous integration on silicon photonics," Proc. IEEE **106**(12), 2258–2269 (2018).
[18] Y. Fan *et al.*, "290 Hz intrinsic linewidth from an integrated optical chip-based widely tunable InP-Si_3N_4 hybrid laser," in *Conference on Lasers and Electro-Optics* (Optical Society of America, San Jose, California, 2017).
[19] A. W. Fang *et al.*, "A racetrack mode-locked silicon evanescent laser," Opt. Express **16**(2), 1393–1398 (2008).
[20] S. Liu *et al.*, "High-channel-count 20 GHz passively mode-locked quantum dot laser directly grown on Si with 4.1 Tbit/s transmission capacity," Optica **6**(2), 128–134 (2019).
[21] W. Sun *et al.*, "Ultra-broadband optical gain in III-nitride digital alloys," Sci. Rep. **8**(1), 3109 (2018).
[22] R. Luo *et al.*, "Semi-nonlinear nanophotonic waveguides for highly efficient second-harmonic generation," Laser Photonics Rev. **13**(3), 1800288 (2019).
[23] M. Belt *et al.*, "Ultra-low-loss Ta_2O_5-core/SiO_2-clad planar waveguides on Si substrates," Optica **4**(5), 532–536 (2017).
[24] T.-J. Lu *et al.*, "Aluminum nitride integrated photonics platform for the ultraviolet to visible spectrum," Opt. Express **26**(9), 11147–11160 (2018).
[25] C. Xiong, W. H. P. Pernice, and H. X. Tang, "Low-loss, silicon integrated, aluminum nitride photonic circuits and their use for electro-optic signal processing," Nano Lett. **12**(7), 3562–3568 (2012).
[26] M. M. Aslan *et al.*, "Low-loss optical waveguides for the near ultra-violet and visible spectral regions with Al_2O_3 thin films from atomic layer deposition," Thin Solid Films **518**(17), 4935–4940 (2010).
[27] C. Sorace-Agaskar *et al.*, "Versatile silicon nitride and alumina integrated photonic platforms for the ultraviolet to short-wave infrared," IEEE J. Sel. Top. Quantum Electron. **25**(5), 1 (2019).
[28] A. Rao and S. Fathpour, "Heterogeneous thin-film lithium niobate integrated photonics for electrooptics and nonlinear optics," IEEE J. Sel. Top. Quantum Electron. **24**(6), 1–12 (2018).
[29] K. Y. Yang *et al.*, "Bridging ultrahigh-Q devices and photonic circuits," Nat. Photonics **12**(5), 297–302 (2018).
[30] D. J. Moss *et al.*, "New CMOS-compatible platforms based on silicon nitride and Hydex for nonlinear optics," Nat. Photonics **7**, 597 (2013).
[31] G. N. West, W. Loh, D. Kharas, C. Sorace-Agaskar, K. K. Mehta, J. Sage, J. Chiaverini, and R. J. Ram, "Low-loss integrated photonics for the blue and ultraviolet regime," APL Photonics **4**, 026101 (2019).
[32] Y. C. Cheng and W. D. Festwood, "Losses in tantalum pentoxide waveguides," J. Electron. Mater. **3**(1), 37–50 (1974).
[33] M. Bickermann *et al.*, "UV transparent single-crystalline bulk AlN substrates," Phys. Status Solidi C **7**(1), 21–24 (2010).
[34] A. Raza *et al.*, "High index contrast photonic platforms for on-chip Raman spectroscopy," Opt. Express **27**(16), 23067–23079 (2019).
[35] Z. Ye *et al.*, "Low-loss high-Q silicon-rich silicon nitride microresonators for Kerr nonlinear optics," Opt. Lett. **44**(13), 3326–3329 (2019).
[36] A. Gorin *et al.*, "Fabrication of silicon nitride waveguides for visible-light using PECVD: A study of the effect of plasma frequency on optical properties," Opt. Express **16**(18), 13509–13516 (2008).

[37]J. F. Bauters *et al.*, "Ultra-low-loss (<0.1 dB/m) planar silica waveguide technology," in *IEEE Photonics Conference* (IEEE, 2011).
[38]T. A. Huffman *et al.*, "Integrated resonators in an ultralow loss Si_3N_4/SiO_2 platform for multifunction applications," IEEE J. Sel. Top. Quantum Electron. **24**(4), 1–9 (2018).
[39]J. F. Bauters *et al.*, "Ultra-low-loss high-aspect-ratio Si_3N_4 waveguides," Opt. Express **19**(4), 3163–3174 (2011).
[40]M. Puckett *et al.*, "Higher order cascaded SBS suppression using gratings in a photonic integrated ring resonator laser," in *Conference on Lasers and Electro-Optics* (Optical Society of America, San Jose, California, 2019).
[41]M. H. P. Pfeiffer *et al.*, "Ultra-smooth silicon nitride waveguides based on the damascene reflow process: Fabrication and loss origins," Optica **5**(7), 884–892 (2018).
[42]K. Luke *et al.*, "Overcoming Si_3N_4 film stress limitations for high quality factor ring resonators," Opt. Express **21**(19), 22829–22833 (2013).
[43]H. Jung *et al.*, "Kerr solitons with Tantala ring resonators," in *Nonlinear Optics (NLO)* (Optical Society of America, Waikoloa Beach, Hawaii, 2019).
[44]R. Y. Chen, M. D. Charlton, and P. G. Lagoudakis, "Chi 3 dispersion in planar tantalum pentoxide waveguides in the telecommunications window," Opt. Lett. **34**(7), 1135–1137 (2009).
[45]R. Y. Chen, M. D. B. Charlton, and P. G. Lagoudakis, "Experimental demonstration of on-chip optical parametric oscillation in planar tantalum pentoxide waveguides," Proc. SPIE **7781**, 778108 (2010).
[46]R. Halir *et al.*, "Ultrabroadband supercontinuum generation in a CMOS-compatible platform," Opt. Lett. **37**(10), 1685–1687 (2012).
[47]N. F. Tyndall *et al.*, "Waveguide-enhanced Raman spectroscopy of trace chemical warfare agent simulants," Opt. Lett. **43**(19), 4803–4806 (2018).
[48]W. Kulisch *et al.*, *Tantalum Pentoxide as a Material for Biosensors: Deposition, Properties and Applications* (Springer, 2009), pp. 509–524.
[49]T. Kessler *et al.*, "A sub-40-mHz-linewidth laser based on a silicon single-crystal optical cavity," Nat. Photonics **6**, 687 (2012).
[50]D. J. Blumenthal, "Ultra-stable integrated lasers and low-cost, low-energy coherent data center interconnect," in *OSA Advanced Photonics Congress (AP) 2019 (IPR, Networks, NOMA, SPPCom, PVLED)* (Optical Society of America, Burlingame, California, 2019).
[51]C. L. Degen, F. Reinhard, and P. Cappellaro, "Quantum sensing," Rev. Mod. Phys. **89**(3), 035002 (2017).
[52]J. Kitching, S. Knappe, and E. A. Donley, "Atomic sensors—A review," IEEE Sens. J. **11**(9), 1749–1758 (2011).
[53]L. C. Sinclair *et al.*, "Compact fiber frequency combs for precision measurement outside the metrology lab," in *Latin America Optics and Photonics Conference* (Optical Society of America, Lima, 2018).
[54]J. Li, H. Lee, and K. J. Vahala, "Microwave synthesizer using an on-chip Brillouin oscillator," Nat. Commun. **4**, 2097 (2013).
[55]J. Li, M.-G. Suh, and K. Vahala, "Microresonator Brillouin gyroscope," Optica **4**(3), 346–348 (2017).
[56]K. O. Hill, B. S. Kawasaki, and D. C. Johnson, "cw Brillouin laser," Appl. Phys. Lett. **28**(10), 608–609 (1976).
[57]R. I. Woodward *et al.*, "Stimulated Brillouin scattering of visible light in small-core photonic crystal fibers," Opt. Lett. **39**(8), 2330–2333 (2014).
[58]S. P. Smith, F. Zarinetchi, and S. Ezekiel, "Narrow-linewidth stimulated Brillouin fiber laser and applications," Opt. Lett. **16**(6), 393–395 (1991).
[59]A. Bartels *et al.*, "Stabilization of femtosecond laser frequency combs with subhertz residual linewidths," Opt. Lett. **29**(10), 1081–1083 (2004).
[60]W. Loh *et al.*, "Ultra-narrow linewidth Brillouin laser with nanokelvin temperature self-referencing," Optica **6**(2), 152–159 (2019).
[61]R. W. P. Drever *et al.*, "Laser phase and frequency stabilization using an optical resonator," Appl. Phys. B **31**(2), 97–105 (1983).
[62]Z. L. Newman *et al.*, "Architecture for the photonic integration of an optical atomic clock," Optica **6**(5), 680–685 (2019).
[63]I. S. Grudinin, A. B. Matsko, and L. Maleki, "Brillouin lasing with a CaF_2 whispering gallery mode resonator," Phys. Rev. Lett. **102**(4), 043902 (2009).
[64]I. V. Kabakova *et al.*, "Narrow linewidth Brillouin laser based on chalcogenide photonic chip," Opt. Lett. **38**(17), 3208–3211 (2013).
[65]N. T. Otterstrom *et al.*, "A silicon Brillouin laser," Science **360**(6393), 1113 (2018).
[66]S. Gundavarapu *et al.*, "Sub-hertz fundamental linewidth photonic integrated Brillouin laser," Nat. Photonics **13**(1), 60–67 (2019).
[67]R. Pant *et al.*, "On-chip stimulated Brillouin scattering," Opt. Express **19**(9), 8285–8290 (2011).
[68]E. A. Kittlaus, H. Shin, and P. T. Rakich, "Large Brillouin amplification in silicon," Nat. Photonics **10**, 463 (2016).
[69]H. Lee *et al.*, "Chemically etched ultrahigh-Q wedge-resonator on a silicon chip," Nat. Photonics **6**(6), 369–373 (2012).
[70]B. J. Eggleton *et al.*, "Brillouin integrated photonics," Nat. Photonics **13**(10), 664–677 (2019).
[71]Editorial, "Rulers of light," Nat. Photonics **13**(3), 137 (2019).
[72]E. S. Lamb *et al.*, "Optical-frequency measurements with a Kerr microcomb and photonic-chip supercontinuum," Phys. Rev. Appl. **9**(2), 024030 (2018).
[73]V. Brasch *et al.*, "Photonic chip–based optical frequency comb using soliton Cherenkov radiation," Science **351**(6271), 357 (2016).
[74]M. H. P. Pfeiffer *et al.*, "Photonic Damascene process for integrated high-Q microresonator based nonlinear photonics," Optica **3**(1), 20–25 (2016).
[75]P. Del'Haye *et al.*, "Optical frequency comb generation from a monolithic microresonator," Nature **450**, 1214 (2007).
[76]T. C. Briles *et al.*, "Interlocking Kerr-microresonator frequency combs for microwave to optical synthesis," Opt. Lett. **43**(12), 2933–2936 (2018).
[77]M.-G. Suh *et al.*, "Searching for exoplanets using a microresonator astrocomb," Nat. Photonics **13**(1), 25–30 (2019).
[78]D. T. Spencer *et al.*, "An optical-frequency synthesizer using integrated photonics," Nature **557**(7703), 81–85 (2018).
[79]D. J. Jones *et al.*, "Carrier-envelope phase control of femtosecond mode-locked lasers and direct optical frequency synthesis," Science **288**(5466), 635 (2000).
[80]P. Marin-Palomo *et al.*, "Microresonator-based solitons for massively parallel coherent optical communications," Nature **546**, 274 (2017).
[81]T. J. Kippenberg *et al.*, "Dissipative Kerr solitons in optical microresonators," Science **361**(6402), eaan8083 (2018).
[82]T. Herr *et al.*, "Temporal solitons in optical microresonators," Nat. Photonics **8**, 145 (2013).
[83]M.-G. Suh *et al.*, "Microresonator soliton dual-comb spectroscopy," Science **354**(6312), 600 (2016).
[84]S. Miller *et al.*, "On-chip frequency comb generation at visible wavelengths via simultaneous second- and third-order optical nonlinearities," Opt. Express **22**(22), 26517–26525 (2014).
[85]X. Liu *et al.*, "Generation of multiple near-visible comb lines in an AlN microring via $\chi(2)$ and $\chi(3)$ optical nonlinearities," Appl. Phys. Lett. **113**(17), 171106 (2018).
[86]X. Guo, C.-L. Zou, H. Jung, Z. Gong, A. Bruch, and L. Jiang *et al.*, "Efficient generation of a near-visible frequency comb via Cherenkov-like radiation from a Kerr microcomb," Phys. Rev. Appl. **10**(1), 014012 (2018).
[87]M. Kues *et al.*, "Quantum optical microcombs," Nat. Photonics **13**(3), 170–179 (2019).
[88]C. Reimer *et al.*, "Integrated frequency comb source of heralded single photons," Opt. Express **22**(6), 6535–6546 (2014).
[89]C. Reimer *et al.*, "Generation of multiphoton entangled quantum states by means of integrated frequency combs," Science **351**(6278), 1176 (2016).
[90]M. Kues *et al.*, "On-chip generation of high-dimensional entangled quantum states and their coherent control," Nature **546**, 622 (2017).
[91]L. G. Helt *et al.*, "Spontaneous four-wave mixing in microring resonators," Opt. Lett. **35**(18), 3006–3008 (2010).
[92]L. A. M. Barea *et al.*, "Photonic molecules for optical signal processing," in *2014 IEEE Photonics Conference* (IEEE, 2014).
[93]S. V. Boriskina, "Photonic molecules and spectral engineering," in *Photonic Microresonator Research and Applications*, edited by I. Chremmos, O. Schwelb, and N. Uzunoglu (Springer, 2010).
[94]M. Pöllinger and A. Rauschenbeutel, "All-optical signal processing at ultra-low powers in bottle microresonators using the Kerr effect," Opt. Express **18**(17), 17764–17775 (2010).

[95]T. Carmon and K. J. Vahala, "Visible continuous emission from a silica microphotonic device by third-harmonic generation," Nat. Phys. **3**(6), 430–435 (2007).
[96]J. Zhu *et al.*, "On-chip single nanoparticle detection and sizing by mode splitting in an ultrahigh-Q microresonator," Nat. Photonics **4**(1), 46–49 (2010).
[97]A. M. Armani *et al.*, "Label-free, single-molecule detection with optical microcavities," Science **317**(5839), 783 (2007).
[98]S. Ishii, K. Nozaki, and T. Baba, "Photonic molecules in photonic crystals," Jpn. J. Appl. Phys., Part 1 **45**(8A), 6108–6111 (2006).
[99]W. Yoshiki *et al.*, "Observation of energy oscillation between strongly-coupled counter-propagating ultra-high Q whispering gallery modes," Opt. Express **23**(24), 30851–30860 (2015).
[100]A. Tomadin and R. Fazio, "Many-body phenomena in QED-cavity arrays," J. Opt. Soc. Am. B **27**(6), A130–A136 (2010).
[101]M. J. Hartmann, F. G. S. L. Brandão, and M. B. Plenio, "Quantum many-body phenomena in coupled cavity arrays," Laser Photonics Rev. **2**(6), 527–556 (2008).
[102]M. T. Hummon *et al.*, "Photonic chip for laser stabilization to an atomic vapor with 10–11 instability," Optica **5**(4), 443–449 (2018).
[103]M. Bayer and A. Forchel, "Confined optical modes in photonic molecules and crystals," in *Advances in Solid State Physics* (Springer Berlin Heidelberg, Berlin, Heidelberg, 2000), Vol. 40.
[104]Y. Zhao *et al.*, "Ultrafast optical switching using photonic molecules in photonic crystal waveguides," Opt. Express **23**(7), 9211–9220 (2015).
[105]M. Bayer *et al.*, "Optical modes in photonic molecules," Phys. Rev. Lett. **81**(12), 2582–2585 (1998).
[106]M. Bayer *et al.*, "Optical demonstration of a crystal band structure formation," Phys. Rev. Lett. **83**(25), 5374–5377 (1999).
[107]S. Haddadi *et al.*, "Photonic molecules: Tailoring the coupling strength and sign," Opt. Express **22**(10), 12359–12368 (2014).
[108]H. Altug and J. Vučković, "Two-dimensional coupled photonic crystal resonator arrays," Appl. Phys. Lett. **84**(2), 161–163 (2004).
[109]Y.-S. Choi *et al.*, "Dispersive phase response in optical waveguide-resonator system," Appl. Phys. Lett. **90**(19), 1108 (2007).
[110]M. Davanço *et al.*, "Detailed characterization of slow and dispersive propagation near a mini-stop-band of an InP photonic crystal waveguide," Opt. Express **13**(13), 4931–4938 (2005).
[111]M. Davanço *et al.*, "Compact broadband photonic crystal filters with reduced back-reflections for monolithic InP-based photonic integrated circuits," IEEE Photonics Technol. Lett. **18**, 1155–1157 (2006).
[112]M. Davanco *et al.*, "Broadband notch filters based on quasi-2-D photonic crystal waveguides for InP-based monolithic photonic-integrated circuits," IEEE J. Sel. Top. Quantum Electron. **12**(6), 1164–1174 (2006).
[113]Y. M. Landobasa and M. K. Chin, "Defect modes in micro-ring resonator arrays," Opt. Express **13**(20), 7800–7815 (2005).
[114]G. Guttroff *et al.*, "Photonic defect states in chains of coupled microresonators," Phys. Rev. B **64**(15), 155313 (2001).
[115]J. P. Epping *et al.*, "Ultra-low-power stress-optics modulator for microwave photonics," Proc. SPIE **10106**, 101060F (2017).
[116]P. R. Stanfield *et al.*, "CMOS-compatible, piezo-optomechanically tunable photonics for visible wavelengths and cryogenic temperatures," Opt. Express **27**(20), 28588–28605 (2019).
[117]K. Alexander *et al.*, "Broadband electro-optic modulation using low-loss PZT-on-silicon nitride integrated waveguides," in *Conference on Lasers and Electro-Optics* (Optical Society of America, San Jose, California, 2017).
[118]R. L. Moreira, "Integrated optical delay line circuits on a ultra-low loss planar waveguide platform," in *Electrical and Computer Engineering* (University of California at Santa Barbara, 2016).
[119]A. Leinse *et al.*, "TriPleX waveguide platform: Low-loss technology over a wide wavelength range," Proc. SPIE **8767**, 87670E (2013).
[120]L. Zhuang *et al.*, "Low-loss, high-index-contrast Si_3N_4/SiO_2 optical waveguides for optical delay lines in microwave photonics signal processing," Opt. Express **19**(23), 23162–23170 (2011).
[121]R. Moreira, S. Gundavarapu, and D. J. Blumenthal, "Compact programmable monolithically integrated 10-stage multi-channel WDM dispersion equalizer on low-loss silicon nitride planar waveguide platform," in *Optical Fiber Communication Conference* (Optical Society of America, 2015).
[122]J. Capmany *et al.*, "Discrete-time optical processing of microwave signals," J. Lightwave Technol. **23**(2), 702–723 (2005).
[123]C. G. H. Roeloffzen, L. Zhuang, R. G. Heideman, A. Borreman, and W. van Etten, "Ring resonator-based tunable optical delay line in LPCVD waveguide technology," in *IEEE/LEOS Symposium Benelux Chapter* (Faculte Polytechnique de Mons Belgium, IEEE LEOS, 2005).
[124]T. Huffman *et al.*, "Ultra-low loss large area waveguide coils for integrated optical gyroscopes," IEEE Photonics Technol. Lett. **29**(2), 185–188 (2017).
[125]S. Gundavarapu *et al.*, "Integrated ultra-low-loss silicon nitride waveguide coil for optical gyroscopes," in *Optical Fiber Communication Conference* (Optical Society of America, 2016).
[126]R. L. Moreira *et al.*, "Integrated ultra-low-loss 4-bit tunable delay for broadband phased array antenna applications," IEEE Photonics Technol. Lett. **25**(12), 1165–1168 (2013).
[127]Cisco, Cisco Global Cloud Index: Forecast and Methodology, 2016–2021 White Paper, 2018.
[128]J. K. Perin, A. Shastri, and J. M. Kahn, "Design of low-power DSP-free coherent receivers for data center links," J. Lightwave Technol. **35**(21), 4650–4662 (2017).
[129]D. J. Blumenthal *et al.*, "Frequency stabilized lasers for coherent fiber interconnects in the datacenter (invited talk)," in *2019 IEEE Optical Interconnects Conference (OI)* (IEEE, 2019).
[130]S. Gundavarapu *et al.*, "Interferometric optical gyroscope based on an integrated Si_3N_4 low-loss waveguide coil," J. Lightwave Technol. **36**(4), 1185–1191 (2018).
[131]S. Srinivasan *et al.*, "Design of integrated hybrid silicon waveguide optical gyroscope," Opt. Express **22**(21), 24988–24993 (2014).
[132]A. Politi *et al.*, "Silica-on-Silicon waveguide quantum circuits," Science **320**(5876), 646 (2008).
[133]N. Chauhan *et al.*, "Photonic integrated Si_3N_4 ultra-large-area grating waveguide MOT interface for 3D atomic clock laser cooling," in *Conference on Lasers and Electro-Optics* (Optical Society of America, San Jose, California, 2019).
[134]C. Monroe *et al.*, "Very cold trapped atoms in a vapor cell," Phys. Rev. Lett. **65**(13), 1571–1574 (1990).
[135]H. J. Metcalf and P. van der Straten, *Laser Cooling and Trapping* (Springer-Verlag, 1999), p. 324.